electronics

MDPI

Article

Multi-Fault Diagnosis of Electric Vehicle Power Battery Based on Double Fault Window Location and Fast Classification

Xiaowei Shen †, Shuxian Lun *,† and Ming Li *

College of Control Science and Engineering, Bohai University, Jinzhou 121013, China; 2021008004@qymail.bhu.edu.cn

* Correspondence: lunshuxian@qymail.bhu.edu.cn (S.L.); lm_dq@bhu.edu.cn (M.L.)

† These authors contributed equally to this work.

Abstract: As energy supply units, lithium-ion batteries have been widely used in the electric vehicle industry. However, the safety of lithium-ion batteries remains a significant factor limiting their development. To achieve rapid fault diagnosis of lithium-ion batteries, this paper presents a comprehensive fault diagnosis process. Firstly, an interleaved voltage sensor topology structure is utilized to acquire battery voltage data. An improved complete ensemble empirical mode decomposition with adaptive noise method is introduced to process data. Then, the reconstructed voltage data sequence is used to eliminate the influence of noise. A fault location is performed using dichotomy correlation coefficient and time window correlation coefficient. Afterwards, principal component analysis is used to select the principal components with high contribution rate as classification features. The gray wolf optimization algorithm is used to find the parameters of the least squares support vector machine, constructing an optimal classifier for fault classification. A fault experiment platform is established to realize the physical triggering of faults such as external short circuit, internal circuit, and connection of experimental battery packs. Finally, the accuracy and reliability of the method are verified by the results of fault localization and fault type determination.

Keywords: electric vehicle; lithium-ion battery; fault diagnosis; fault location

check for updates

Citation: Shen, X.; Lun, S.; Li, M. Multi-Fault Diagnosis of Electric Vehicle Power Battery Based on Double Fault Window Location and Fast Classification. *Electronics* **2024**, *13*, 612. https://doi.org/10.3390/electronics13030612

Academic Editor: Felipe Jiménez

Received: 30 November 2023
Revised: 17 January 2024
Accepted: 26 January 2024
Published: 1 February 2024

Copyright: © 2024 by the authors. Licensee MDPI, Basel, Switzerland. This article is an open access article distributed under the terms and conditions of the Creative Commons Attribution (CC BY) license (https://creativecommons.org/licenses/by/4.0/).

1. Introduction

In recent years, the increasing concern regarding global warming and the rising price of fossil energy have forced the automotive industry to pay close attention to economic and emission reduction topics. As a new development trend, electric vehicles are occupying the mainstream in the transportation industry by virtue of their advantages of environmental protection, energy saving, and low cost. At the same time, the lithium-ion battery is widely used in new energy vehicles, given its high energy/power density, extended cycle life, etc. However, in recent years, owing to the failure of lithium-ion batteries, spontaneous combustion and explosion accidents of electric vehicles have occurred frequently. In the field of energy-based maintenance (EBM), the safety of lithium-ion battery systems has received considerable attention [1,2]. Through the battery management system (BMS), the lithium-ion battery can be monitored, and the collected data can be processed and analyzed to achieve the management of the lithium-ion battery. When an abnormal state of the battery cell is found, the BMS will quickly sound an alarm to prevent the occurrence of safety accidents [3–6]. Nevertheless, BMS can not detect all kinds of faults of Li-ion batteries, so exploring new fault diagnosis methods is an important research direction in the field of EBM.

The faults of lithium-ion batteries are divided into short circuit faults, abuse faults, contact faults, and sensor faults. The short circuit fault of the lithium-ion battery is divided into external short circuit (ESC) [7] and internal short circuit (ISC) [8–10]. The ESC fault releases a lot of heat in a very short time, which can easily cause a fire. The ISC fault is not obvious at the early stage of the fault, but will deteriorate rapidly with time, and

eventually lead to the ESC fault. At the same time, the abuse of a lithium-ion battery, such as thermal abuse, mechanical abuse, and electrical abuse, will cause irreversible damage to the lithium-ion battery, which not only reduces the performance of the lithium-ion battery, but also increases the possibility of ISC fault [11]. Secondly, due to the defects of the production process and improper connection of lithium-ion batteries, the increase in the resistance of the connection points between lithium-ion batteries affects the thermal safety and aging speed of lithium-ion batteries [12,13]. In addition, the sensor in the battery system fails unexpectedly, which leads to inaccurate data obtained by the battery management system, and then gives wrong response measures. So the safety of lithium-ion batteries remains an obstacle to further development. In addition, as a chemical power source, a lithium-ion battery is easily affected by the external environment, leading to its highly nonlinear characteristics, which brings challenges to the fault diagnosis process of lithium-ion batteries [14].

Safety issues of lithium-ion batteries have attracted significant attention recently, with a significant amount of work dedicated to fault detection and diagnosis. These methods can be roughly divided into two categories: model-based diagnostic methods and model-free diagnostic methods. The model-free diagnostic methods include knowledge-based diagnostic methods and data-driven diagnostic methods.

The model-based fault diagnosis method usually involves building equivalent circuit models or electrochemical models of lithium-ion batteries [15,16]. The model-based diagnostic method accurately describes the internal state of the system and is effective for diagnosing single fault systems. Yu et al. [17] established a diagnostic model combining voltage parameters and current parameters. They combined the least square method with the unscented Kalman filter to predict the fault current, and compared it with the current threshold to judge the fault. Wei et al. [18] put forward an electrothermal coupling model based on the battery electrical and thermal dynamic behavior, combined with the battery internal resistance estimator based on Lyapunov to diagnose thermal abuse faults. A model using the real charging state and estimated charging state residual was proposed by Xiong et al. [19], and they use a threshold to diagnose sensor faults. A model observer based on partial differential equations was proposed by Dey et al. [20] and the threshold limit and Lyapunov stability theory were to judge the thermal failure of lithium-ion batteries. The model-based fault diagnosis method has the advantages of high efficiency and accuracy. However, the method is unable to diagnose multiple fault problems due to inconsistencies between lithium-ion batteries and identification parameter problems.

The knowledge-based diagnosis method depends on the characteristics of the experimental object, namely the lithium-ion battery system itself [21]. Knowledge-based diagnosis methods include many algorithms, such as expert system theory and fuzzy logic rule judgment. With the understanding of the operating mechanism of the experimental object, a large amount of knowledge and experience are accumulated to help establish the mapping relationship between various faults and data characteristics. This method can provide clear fault diagnosis interpretation and requires less data support. In the available literature, many people have used this method. Wu et al. [22] proposed a fuzzy logic diagnosis method for overcharge, over-discharge, and heat abuse faults by taking advantage of changes in electrical parameters and capacity parameters. The knowledge-based fault diagnosis method is often combined with battery models and relies on historical data. However, this method not only has difficulty in obtaining a large amount of historical data, but also relies heavily on the prior knowledge of expert systems. Furthermore, it is relatively difficult to update and maintain the knowledge base when establishing the expert system. Therefore, the knowledge-based fault diagnosis method is effective in fault detection but hindered by factors such as historical data and subjective selection.

The data-driven diagnosis method mainly uses the real-time data of BMS to judge and classify battery faults [23]. The voltage correlation coefficient method based on the recursive moving time window was put forward by Xia et al. [24,25] to identify the battery short circuit faults. Meanwhile, the staggered voltage measurement method was proposed for the

battery topology to realize the accurate location of the faulty battery and set the threshold to identify the battery fault. Kang et al. [26,27] proposed a cross-measurement topology for battery packs and realized multiple fault diagnosis by using an improved correlation coefficient method. Yang et al. [28] used the principal component analysis algorithm to extract data features and the correlation vector machine to realize the classification of data features, so as to complete the classification of battery faults and fault degree. Zhou et al. [29] used various types of neural networks to diagnose power battery faults and output fault types. The fault method of lithium-ion batteries based on the isolated forest algorithm was proposed by Jiang et al. [30], and the variational mode decomposition algorithm was used for data preprocessing, finally realizing the multi-fault diagnosis of lithium-ion batteries. Ma et al. [31] used the contribution degree of principal component analysis to judge the abnormal data, and used kernel principal component analysis to reconstruct the battery parameters and compared them with the normal parameters to achieve fault classification. Xu et al. [32] extracted the data features of the simulation model and used decision tree and cloud algorithm to judge the fault classification. The data-driven diagnosis method has the merits of strong adaptability, low cost of update learning, and high robustness. In fact, noise in the measurement data and inconsistencies between the cells can cause the final data to not accurately reflect the actual state of the battery. In addition, high demands on data quality and black boxes in the diagnostic process all can affect the accuracy and readability of data-driven methods. In summary, the data-driven fault diagnosis method requires neither the creation of multiple algorithms for different faults nor the support of large amounts of historical data, and it improves the speed and accuracy of fault diagnosis.

Based on previous research, a fault location and classification method for lithium-ion battery pack based on double fault windows and least squares support vector machine-grey wolf optimization (GWO-LSSVM) algorithm is proposed in this paper. Firstly, in the aspect of data preprocessing for the given analysis, the data sequence is decomposed by an improved complete ensemble empirical mode decomposition with adaptive noise (ICEEMDAN), and we reconstruct the data sequence. In addition, the correlation coefficient method based on dichotomy and the correlation coefficient method based on time window are designed to identify fault location principal component analysis (PCA), which is used to reduce the dimension of the decomposed intrinsic mode functions (IMFs), and the fault characteristics are determined by the contribution degree. Finally, the parameters of the least square support vector machine (LSSVM) are confirmed by the grey wolf optimization (GWO) algorithm, and the fault classification is realized. The main contributions of this paper are as follows:

1. Building a fault experiment platform, testing the fault, and recording the voltage data.

2. A double fault window location method based on dichotomy correlation coefficient and time window correlation coefficient is proposed to effectively judge the fault window, reducing the calculation cost of fault location and improving efficiency.

3. Considering the data noise and the inconsistency between batteries, the model has good robustness.

The structure of this paper is as follows. Section 2 describes the experimental content, and the experimental platform and experimental methods are described. In Section 3, the lithium-ion battery fault location and fault classification methods are introduced in detail. In order to verify the effectiveness of the proposed scheme, the performance of the corresponding method for the fault classification problem of lithium-ion batteries is discussed in Section 4. The conclusion is given in Section 5.

2. Experiment

2.1. Sudden Fault and Progressive Fault

Progressive fault refers to faults in which battery performance gradually degrades over a long period of time due to internal reactions and external environments of lithium-ion batteries, such as contact fault. Progressive fault will cause a lithium-ion battery's internal resistance to increase, in addition to electrolyte loss and other problems. This type of fault takes a long time to reach the runaway threshold and has a small impact on battery performance before reaching the runaway threshold. Furthermore, when the fault stops, there is a possibility of self-recovery. Sudden fault refers to a fault that causes lithium-ion batteries to suddenly fail or decline sharply in a period time, including ESC fault, ISC fault, etc. This type of fault cannot heal itself and can quickly cause thermal runaway, triggering spontaneous combustion of the battery. From the time series, progressive fault and sudden fault are two consecutive stages, and progressive fault will eventually cause sudden fault.

2.2. Build Experimental Platform

As shown in Figure 1, the experimental platform consists of a lithium-ion battery pack, battery test system, fault injection device, and data processing equipment. A battery pack consisting of four lithium-ion batteries (lithium-ion polymer battery, 5000 mAh, standard voltage 3.7 V) connected in series was used as the experimental subject. The battery test system acts as a power load and it is responsible for collecting voltage data. A fault injection device is used to inject a fault into the battery pack. The data processing equipment processes the voltage data collected by the BTS. The battery test system performs a dynamic stress test (DST) on the experimental battery cells at room temperature. The first battery test system, model C1-4001-60V100A-NA, is employed to simulate the dynamic load experienced by the battery pack during use. The second battery test system, model C1-8004-5V200A-NIFA, was used to collect voltage data of the battery pack with a sampling frequency of 10Hz and a voltage range of 0∼5 V. The fault injection device consists of the STM32F103RCT6 microprocessor and relay. The experimental cell information is shown in Table 1.

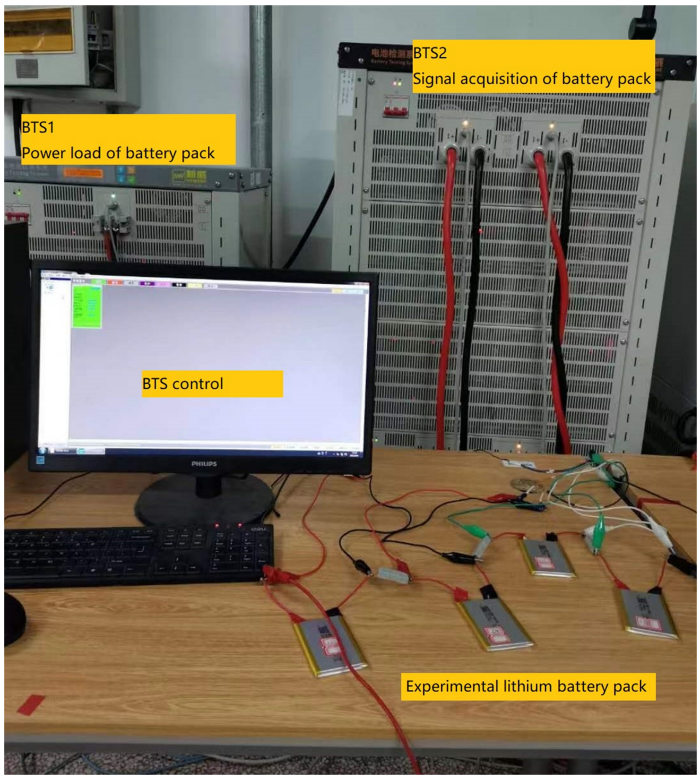


Figure 1. Lithium-ion battery pack experimental platform.

Table 1. Specifications of the ternary lithium-ion battery used in the experiment.

Lithium-Ion Battery Index	Parameter
Nominal capacity/Ah	5
Rated voltage/V	3.7
Charging cut-off voltage/V	4.2
Discharge cut-off voltage/V	2.75
Standard charging current/A	2.5
Standard discharge current/A	2.5
Maximum charging current/A	5
Maximum discharge current/A	5
Discharge temperature/°C	−35–60

2.3. Burst Fault Injection Experiment

2.3.1. External Short Circuit Test

The cause of the ESC fault is an accidental shorting of the battery's positive and negative terminals. In general, accidental damage to the battery case, battery impact, and errors in the use of the battery may cause the battery to be shorted and lead to ESC fault. In addition, the ESC fault of the battery has serious consequences. Either long-term fault or short-term fault will cause irreversible damage to the lithium-ion battery, and may even lead to fire. Therefore, under the premise of ensuring the safety of the experiment, a metal resistor of 10 milliohms is connected in parallel at both ends of a battery, and the ESC fault of different degrees is simulated by changing the time of the short circuit experiment. The test data of ESC fault are shown in Table 2.

Table 2. ESC fault test parameters.

Fault Degree	Short Circuit Time (ms)
I	100
II	300
III	500

2.3.2. Internal Short Circuit Test

The ISC fault is more concealed than the ESC fault, and has the characteristics of irreversibility and fault accumulation. Impact, puncture, overcharging, and over-discharging methods are often used to simulate ISC fault. The above methods are destructive experiments, and it is difficult to control the corresponding parameter changes and quantify the fault degree during the experiment, and there is an uncontrollable risk. Therefore, a metal resistor is connected in parallel with both ends of a specific battery in the battery pack. By adjusting the resistance value of the metal resistor, ISC fault of varying degrees can be simulated. The test data for ISC fault are presented in Table 3.

Table 3. ISC fault test parameters.

Fault Degree	Short Circuit Resistanc (Ω)
I	1
II	2
III	5

2.4. Persistent Fault Injection Experiment

The connection failure is usually caused by the vibration of the lithium-ion battery during use or the non-standard operation during the connection. A faulty connection will lead to an increase in resistance at the connection and abnormal fluctuations in battery voltage, resulting in additional losses. Unlike short circuit faults, connection faults are reversible faults. In injecting this fault, metal resistors of different resistance values were

used in series with the experimental cells to represent different degrees of connection fault. The experimental data of connection fault are shown in Table 4.

Table 4. Contact fault test parameters.

Fault Degree	Series Resistance (mΩ)
I	20
II	50
III	100

3. Fault Location and Classification Methods

3.1. Voltage Correlation Coefficient

As shown in Figure 2, the batteries are connected in series by wires. In order to identify sensor faults, staggered voltage sensors are used to collect the voltage of each part of the battery pack. Battery faults are different from sensor faults. When C_n of a battery string is faulty, abnormal data are collected by the adjacent voltage sensors $V_{(n-1)}$ and V_n. The measurement data from other voltage sensors remain unaffected. When voltage sensor V_n is faulty, the batteries in the battery string are not affected [24,25]. The adjacent voltage sensors $V_{(n-1)}$ and V_n collect normal data. The Pearson correlation coefficient is defined as follows :

$$r(x,y) = \frac{\mathrm{cov}(x,y)}{\sigma x \cdot \sigma y} \tag{1}$$

where $r(x,y)$ is x and y of Pearson's correlation coefficient, $cov(x,y)$ is the covariance of x and y, and σx and σy are the standard deviations of x and y, respectively.

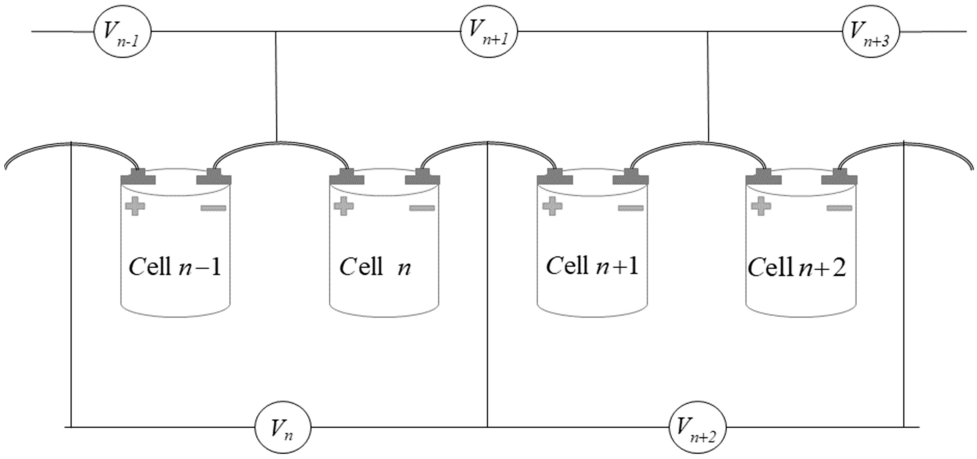


Figure 2. The voltage sensor topology for the pack.

In an ideal state, since the working state and working process of the series battery are the same, the variation trend of the battery voltage is also the same, so the correlation coefficient of each voltage sensor value should be 1. However, under normal operation, the difference between charge state and health state will inevitably lead to inconsistency between batteries, and the correlation coefficient of adjacent voltage sensors is close to 1, but not equal to 1. Assume that the voltage sensor collects the voltage sum of two adjacent batteries, and only one of the adjacent batteries fails. By calculating the correlation coefficients of $r(V_{(n-1)}, V_n)$ and $r(V_n, V_{(n+1)})$, battery faults and voltage sensor faults are distinguished. If $r(V_{(n-1)}, V_n)$ and $r(V_n, V_{(n+1)})$ are not close to 1, then it proves V_n voltage sensor fault. If the value of $r(V_{(n-1)}, V_n)$ is close to 1, and the value of $r(V_n, V_{(n+1)})$ is not close to 1, then the C_n of the battery is faulty.

Similarly, when the measurement range of the voltage sensor is expanded, the above judgment rule is still applicable. When the number of batteries collected by the voltage sensor is N, the correlation coefficient method is used to compare the correlation coefficients of the values of N adjacent voltage sensors successively. Because voltage sensor failure and battery failure have different effects on the battery voltage trend, the fault type can be easily identified.

3.2. Improved Complete Ensemble Empirical Mode Decomposition with Adaptive Noise

In practical situations, the failure of lithium-ion batteries or various kinds of mechanical abuse, thermal abuse, etc., will lead to abnormal voltage change data. However, in the early stages of abuse and failure, the voltage changes reflecting the battery status information are very weak and difficult to distinguish. In addition, in the measurement of lithium-ion battery voltage, noise is often caused by mechanical oscillation, instrument drift, and other factors, which will greatly affect the analysis and extraction accuracy of lithium-ion battery voltage data, and even lead to data distortion. In view of the above problems, voltage data should be decomposed to eliminate noise and save fault information.

Empirical mode decomposition (EMD) was proposed to solve the trend term problem of signal data [33]. Compared with the wavelet analysis method, EMD performs signal decomposition according to the time scale characteristics of data itself, without setting the basis function in advance. As a signal processing method in the time-frequency domain, EMD is essentially a means to stabilize non-stationary signals. The wave and trend of different scales in the signal are decomposed step by step to produce a series of data sequences with different characteristic scales, which are called IMF. In order to solve the spurious components and mode aliasing in EMD, the ICEEMDAN [34,35] method is used. In the process of signal processing, ICEEMDAN adds Gaussian white noise processed by EMD decomposition. Then, the residual and IMFs are obtained. The ICEEMDAN decomposition process of the original voltage data is as follows.

White noise is added to the original signal to obtain a new signal.

$$\beta_0 = \frac{\varepsilon_0 std(x)}{std\left(E\left(w^{(i)}\right)\right)} \tag{2}$$

where β_0 is the system parameter, ε_0 is the estimated parameter, x is the original signal, $E_k(\cdot)$ denotes k-order modal components generated by EMD decomposition, $w^{(i)}$ denotes the i-th white noise to be added.

$$x^{(i)} = x + \beta_0 E\left(w^{(i)}\right) \tag{3}$$

where $x^{(i)}$ represents signal data after white noise is added.

$$r_1 = N(x^{(i)}) \tag{4}$$

where r_1 represents the first residual value. The local mean of the resulting signal is denoted by $N(\cdot)$.

$$c_1 = x - r_1 \tag{5}$$

where c_1 is the first IMF value. Then, the second IMF value can be calculated by $c_2 = r_1 - r_2$, and $r_2 = \frac{1}{N}\sum_{i=1}^{N} M\left(r_1 + \beta_1 E\left(w^{(i)}\right)\right)$.

Similarly, according to $c_k = r_{k-1} - r_k$, where $r_k = \frac{1}{N}\sum_{i=1}^{N} M\left(r_{k-1} + \beta_{k-1} E_k\left(w^{(i)}\right)\right)$, the k-th IMF value can be calculated.

Through the above steps, the signal decomposition of ICEEMDAN is realized. Furthermore, ICEEMDAN can only be used when residual components can be decomposed by EMD.

3.3. Double Fault Window Location Method Based on Correlation Coefficient

3.3.1. Fault Window Location Based on Dichotomy

In the long-term test experiment, a large amount of battery pack text data is accumulated, but the sudden faults of the battery pack will happen in a very short time and lead to the rapid deterioration of the health of the faulty battery. Therefore, locating the fault window from a large amount of test data is the key to detecting sudden faults. Dichotomy is a kind of efficient search algorithm which can find the specific interval data in a large amount of data efficiently. Each comparison halves the search area, so the failure window can be quickly located. In addition, since the length of the data is unknown, the length of the fault interval is set as the condition of termination dichotomy. The fault window is defined as the actual fault data length, and the maximum fault window is the fault interval.

3.3.2. Fault Window Locating Based on Time Window

A time window is often used in data segmentation. The length of the time window dictates the sensitivity to voltage changes. A smaller time window results in higher sensitivity, while a larger time window leads to lower sensitivity. A suitable time window can find the fault location under the premise of inconsistent lithium-ion batteries. For the contact fault data that cannot be distinguished by dichotomy, the time window method is used to divide the fault data, and the correlation coefficient of each time window is calculated in turn to diagnose the fault window.

3.4. Principal Component Analysis

PCA is a commonly used data dimensionality reduction algorithm. The algorithm not only transforms high-dimensional data into low-dimensional data, but also preserves as much information as possible. The basic idea of PCA is to map the original data to a new coordinate system by linear transformation, so that the data in the new coordinate system have the maximum variance. In this way, dimensionality reduction is achieved by retaining the principal components of the largest variance. Principal components are the projections of the original data in the new coordinate system, and they are the directions that best represent the data distribution in the original data.

When the number of samples and indicator variables are p and q, the raw data are first normalized to $\tilde{x}_{mn}$. This process calculates the mean and standard deviation by column using a formula to obtain standardized data.

$$\begin{cases} \bar{x}_j = \frac{\sum_{i=1}^{p} x_{ij}}{p} \\ s_j = \sqrt{\frac{\sum_{i=1}^{p} (x_{ij} - \bar{x}_j)^2}{p-1}} \; i = 1, 2 \cdots p. j = 1, 2 \cdots q \\ \tilde{x}_{mn} = \frac{x_{mn} - \bar{x}_n}{s_n} \end{cases} \tag{6}$$

Then, the principal component consists of $R = (r_{ij})$.

$$r_{ij} = \frac{\sum_{k=1}^{p} \tilde{x}_{ki} * \tilde{x}_{kj}}{p-1} \tag{7}$$

Finally, assuming λ is the eigenvalue, the cumulative contribution rate of z principal components, denoted as a_z, is represented as follows:

$$a_z = \frac{\sum_{k=1}^{z} \lambda_k}{\sum_{k=1}^{p} \lambda_k} \; z = 1, 2, \cdots p \tag{8}$$

3.5. Grey Wolf Optimization Algorithm

The GWO algorithm is an intelligent optimization algorithm proposed by Mirjalili et al. [36] based on the social behavior and hunting behavior of gray wolves. As shown in Figure 3, the gray wolf pack is divided into four classes: α, β, δ, and ω. α wolves are the highest leader in the grey wolf population and have the highest decision-making power on hunting, habitat selection, and other activities in the grey wolf population. The secondary leaders of the grey wolf population are the β wolves, whose main job is to assist α wolves' management and also manage the activities of the rest of the pack. δ wolves are watchdogs in the gray wolf population, whose main job is to scout out the boundaries of the pack, warn them of danger, and care for weak and injured wolves. ω wolves are the lowest wolves in the grey wolf population. They obey the other three kinds of wolves in terms of leadership, and make great contribution to the balance and reproduction of the grey wolf population. In hunting, first, gray wolves seek and pursue prey. Second, they chase and harass prey. Then, they attack prey, and finally they capture prey.

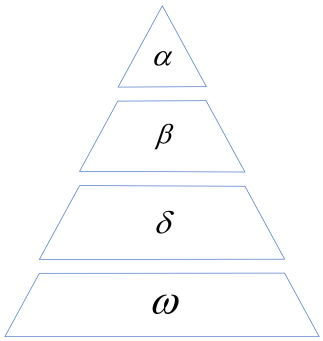


Figure 3. Hierarchy of grey wolf population.

GWO establishes a mathematical model according to the social hierarchy of the grey wolf. The first three optimal solutions correspond to the first three classes of the wolf group, α, β, and δ. The ω wolves are called a candidate solution, and the position is updated according to α, β, and δ.

In the grey wolf optimization algorithm, gray wolves use the following position update formula to surround prey during hunting:

$$\vec{D} = |\vec{C} \cdot \vec{X}_p(t) - \vec{X}(t)| \tag{9}$$

$$\vec{X}(t+1) = \vec{X}_p - \vec{A} \cdot \vec{D} \tag{10}$$

where $\vec{X}_p$ and $\vec{X}$ are the position vector of the prey and the position vector of the gray wolf, respectively, and t is the current iteration number. $\vec{A}$ and $\vec{C}$ are definite coefficients, calculated as follows:

$$\vec{A} = 2 \cdot \vec{a} \cdot \vec{r}_1 - \vec{a} \tag{11}$$

$$\vec{C} = 2 \cdot \vec{r}_2 \tag{12}$$

where $\vec{r}_1$ and $\vec{r}_2$ are two random number vectors with one-dimensional components in [0,1], $\vec{A}$ is used to simulate the attack behavior of gray wolves on prey, and its value is affected by $\vec{a}$. The convergence factor $\vec{a}$ is a key parameter to balance the exploration and development capability of GWO. The value decreases linearly from 2 to 0 as the number of iterations increases.

$$\begin{cases} \vec{D}_\alpha = |\vec{C}_1 \cdot \vec{X}_\alpha - \vec{X}| \\ \vec{D}_\beta = |\vec{C}_2 \cdot \vec{X}_\beta - \vec{X}| \\ \vec{D}_\delta = |\vec{C}_3 \cdot \vec{X}_\delta - \vec{X}| \end{cases} \tag{13}$$

where the positions $\vec{X}_\alpha$, $\vec{X}_\beta$, $\vec{X}_\delta$ of α, β, and δ are updated using the above equation for all gray wolves. $\vec{D}_\alpha$, $\vec{D}_\beta$, and $\vec{D}_\delta$, are the distances of gray wolves from α, β, and δ wolves, respectively. In the iterative process, α, β, and δ are used to guide the movement of ω, thus achieving global optimization.

$$\begin{cases} \vec{X}_1 = \vec{X}_\alpha - \vec{A}_1 \cdot \vec{D}_\alpha \\ \vec{X}_2 = \vec{X}_\beta - \vec{A}_2 \cdot \vec{D}_\beta \\ \vec{X}_3 = \vec{X}_\delta - \vec{A}_3 \cdot \vec{D}_\delta \end{cases} \tag{14}$$

$$\vec{X}(t+1) = \frac{X_1 + X_2 + X_3}{3} \tag{15}$$

where in $\vec{X}_1$, $\vec{X}_2$, and $\vec{X}_3$, respectively, represent the positions of individual ω wolves that need to be adjusted under the influence of wolf pack α, wolf pack β, and wolf pack δ. Here, the average value $\vec{X}(t+1)$ represents the final position.

3.6. Least Squares Support Vector Machine

The Least Squares Support Vector Machine is an improved algorithm based on the support vector machine (SVM) framework. LSSVM changes the hinge loss function used in SVM to solve the empirical risk value, simplifies the inequality constraints in SVM, simplifies them into equality constraints, and reduces the complexity of the solution process of the Lagrange multiplier. The quadratic programming problem in SVM is transformed into solving a system of linear equations, which reduces the computation and complexity of the algorithm.

$$f(x) = \omega^T \Phi(x) + b \tag{16}$$

The formula is the nonlinear optimal classification function of LSSVM; ω^T is the weight vector of the space, and b is the offset. Define the sample dataset $D = \{(x_j, y_j)|j = 1, 2, \cdots n\}$, where $x_j \in R^n$, $y_j \in R^n$, and the sample dataset D is mapped to a high-dimensional space by a nonlinear transformation function $\Phi(x)$.

$$\begin{cases} \min J(\omega, e) = \frac{1}{2}\|\omega\|^2 + \frac{1}{2}\gamma \sum\limits_{i=1}^{N} e_j^2 \\ \text{s.t. } \gamma_j = \omega^T \Phi(x_j) + b + e_j \, j = 1, 2, \cdots m \end{cases} \tag{17}$$

The above formula is the constraint condition of LSSVM, where J represents the optimization function, γ represents the penalty factor, and e_j represents the i error variable.

$$L(\omega, b, e, \alpha) = J(\omega, e) - \sum_{i=1}^{N} \alpha_j \left\{ \omega^T \Phi(x) + b + e_j - y_j \right\} \tag{18}$$

The formula is defined by the Lagrange function.

$$\begin{cases} \frac{\partial L}{\partial \omega} = 0 \Rightarrow \omega = \sum\limits_{i=1}^{N} \alpha_j \Phi(x_j) \\ \frac{\partial L}{\partial b} = 0 \Rightarrow \sum\limits_{i=1}^{N} \alpha_j = 0 \\ \frac{\partial L}{\partial e_j} = 0 \Rightarrow a_j = \gamma e_j \\ \frac{\partial L}{\partial \alpha_j} = 0 \Rightarrow y_j = \omega \Phi(x_j) + b + e_j \end{cases} \tag{19}$$

The partial derivatives of ω, b, e_j, and α_j are calculated.

$$\begin{bmatrix} 0 & \alpha^T \\ \alpha & \Omega + \gamma^{-1} I \end{bmatrix} \begin{bmatrix} b \\ \alpha \end{bmatrix} = \begin{bmatrix} 0 \\ y \end{bmatrix} \tag{20}$$

Eliminating ω and e_j in the formula gives another formula. In that formula, $\alpha = [1, 1 \cdots 1]^T$, $\Omega = \Phi(x_j)^T(x_j)$, $y = [y_1, y_2 \cdots y_m]^T$.

$$y(x) = \sum_{i=1}^{N} \alpha_j K(x, x_i) + b \tag{21}$$

In the formula, $K(x, x_i)$ is the kernel function, and the radial basis function is usually chosen. σ is the undetermined width parameter of the radial basis kernel function.

$$K(x, x_i) = \exp(-\frac{|x - x_i|^2}{2\sigma^2}) \tag{22}$$

3.7. Fault Diagnosis Thought

As shown in Figure 4, the process of battery pack fault diagnosis is divided into three parts: data preprocessing, data feature processing, and fault type classification. The data preprocessing process includes ICEEMDAN decomposition and fault window location. The original voltage data of the battery pack undergo decomposition by ICEEMDAN, with the IMFs and residual terms being retained and reconstructed. The fault location is determined by the double fault window location method. Processing data features involves taking the IMFs as fault features and using PCA to reduce the feature dimension. The process of inputting the reduced-dimension fault features into GWO to find the LSSVM parameters and construct the optimal GWO-LSSVM classifier is called the fault type classification process.

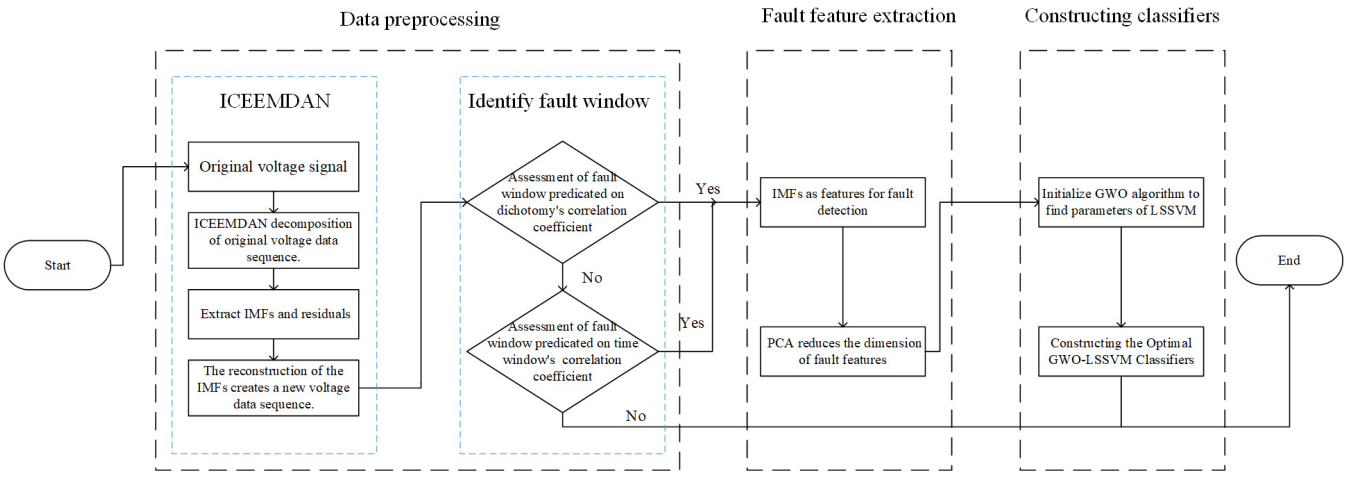


Figure 4. Flow chart of fault location and fault classification.

4. Results and Discussion

4.1. Experimental Data Preprocessing

4.1.1. Data Reconstruction

Due to the topology of the voltmeter interconnection, the voltage data of the lithium-ion battery obtained by the experimental platform are the voltage sum of two lithium-ion batteries. Fault data are concealed within the original data, and the presence of data superposition and noise further complicates the detection of abnormal data. Therefore, ICEEMDAN is employed to process the normal voltage data signal, ESC fault data signal, ISC fault data signal, and contact fault data signal, saving the decomposed IMFs and

residual term. Under the experimental condition that the sampling frequency is 10Hz, ESC fault, ISC fault, and contact fault occur in locations shown in Figure 5. It can be seen from Figure 6 that the ICEEMDAN method decomposes the original signal from high to low frequency into a series of IMF components. Each IMF component is independent and contains different frequency components. The correlation coefficient between each IMF and the original voltage data sequence is calculated using the correlation coefficient method. The IMF with a non-negative correlation coefficient is selected to be accumulated with the residual term, forming a new voltage data sequence. This process can eliminate the effect of noise on the experimental data as much as possible.

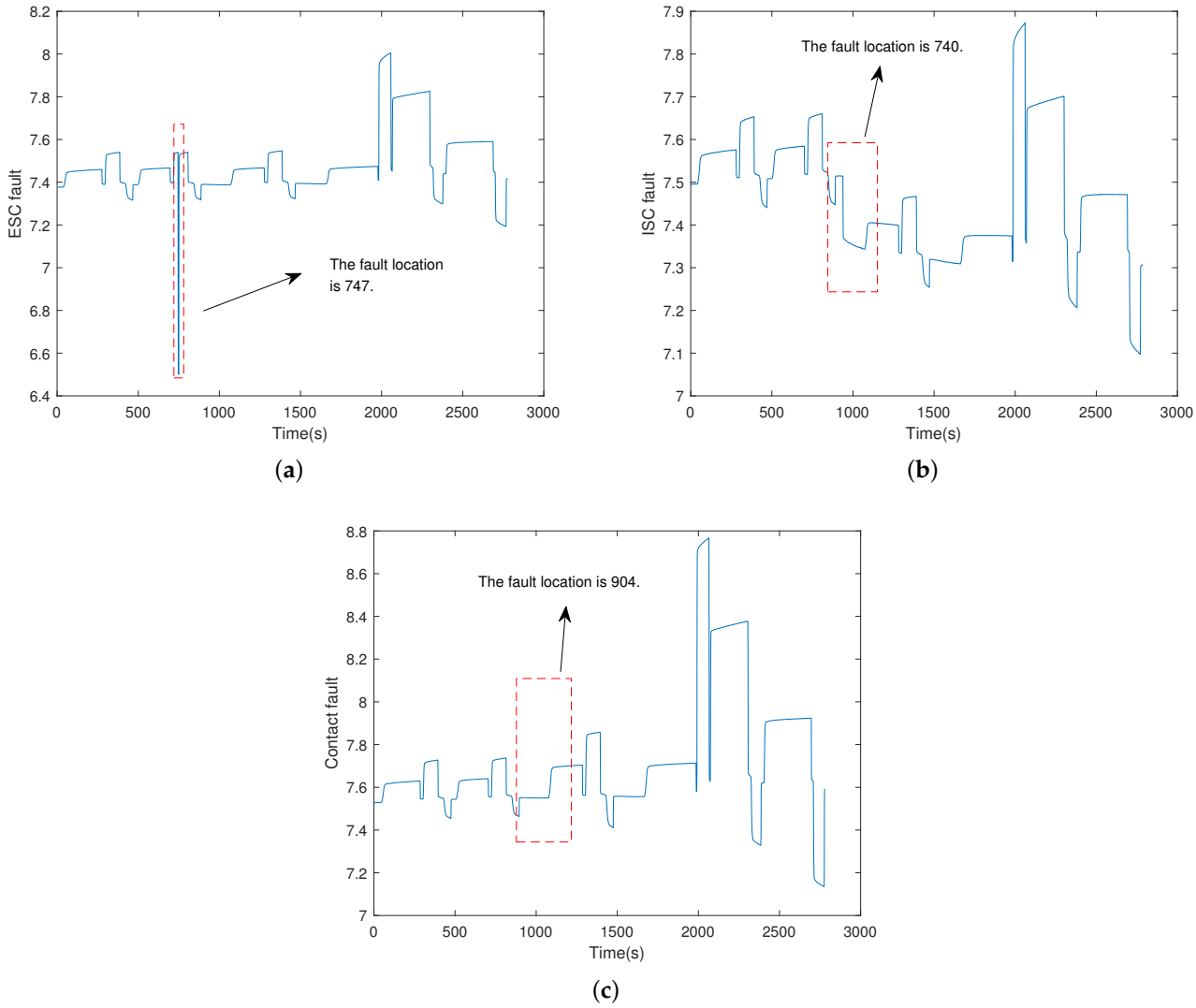


Figure 5. The faults' occurrence position. (**a**) The ESC fault occurrence position; (**b**) the ISC fault occurrence position; (**c**) the contact fault occurrence position.

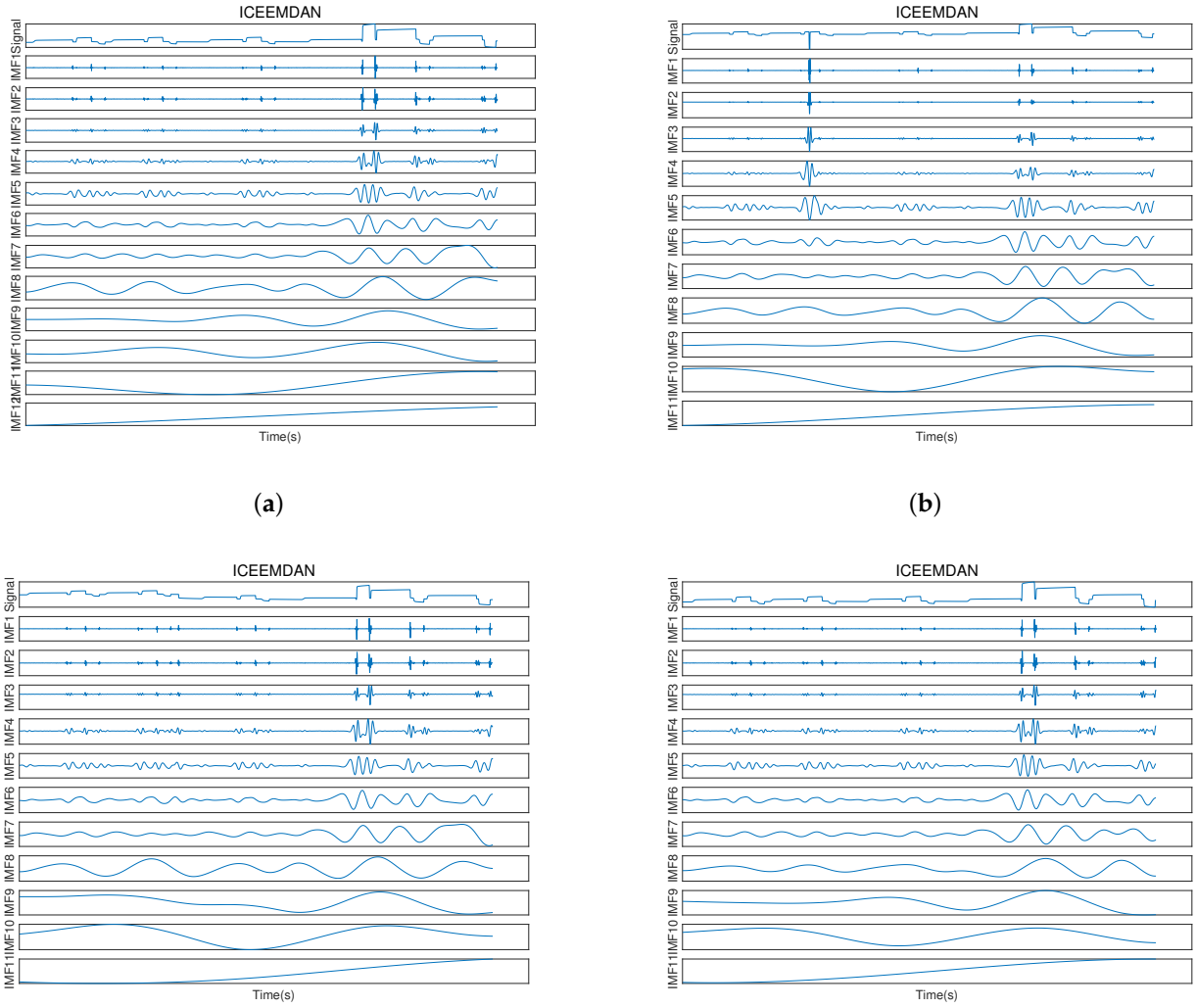


Figure 6. ICEEMDAN decomposition of original voltage signal data. (**a**) Decomposition result of normal voltage signal; (**b**) decomposition result of ESC fault signal; (**c**) decomposition result of ISC fault signal; (**d**) decomposition result of contact fault signal.

4.1.2. Fault Window

Due to the different fault behaviors of ESC fault, ISC fault, and contact fault, the fault location methods used are also different. In order to find the fault window quickly, the double fault window localization method is introduced and the size of the fault window indicates the number of samples. Figures 7 and 8 are the correlation coefficients of the ESC fault and the ISC fault calculated by dichotomy. When the fault window is set to 40, 80, and 120, the number of comparisons decreases in turn. However, the trend of correlation coefficients remains essentially unchanged. The variation in the failure window does not impact the high sensitivity of the correlation coefficient to the failure data. Figure 9 shows the contact fault correlation coefficient calculated through the time window. When the time windows are, respectively, set to 40, 80, and 120, the sensitivity of these different time windows to fault data varies. The smaller the time window, the more sensitive it is to voltage changes, leading to a higher likelihood of misjudgment. However, when the time window is larger, its sensitivity to voltage changes decreases, resulting in an inability to distinguish between failure data and normal data. Therefore, the dichotomy-based correlation coefficient method is employed to diagnose the fault location of both ESC and

ISC fault, with the length of the fault window selected as 80. The correlation coefficient method based on time window is employed to diagnose the location of contact fault, with the length of the time window selected as 80.

4.2. Fault Feature Processing

Although some fault features are reserved in IMFs, there are a large number of data features with low contribution, which will lead to resource waste and uncertainty of diagnosis results in the classification process. Therefore, PCA is used to reduce the dimension of IMFs. Cumulative contribution rate is the proportion of the total variance explained by the top N principal components to the total variance. It is generally believed that when the cumulative contribution rate of principal components reaches 90%, it means that most of the information in the original data has been captured. As shown in Figure 10, the cumulative contribution rate of the first six principal components is about 90%, so the first six principal components are selected as the input fault characteristics of the classification model.

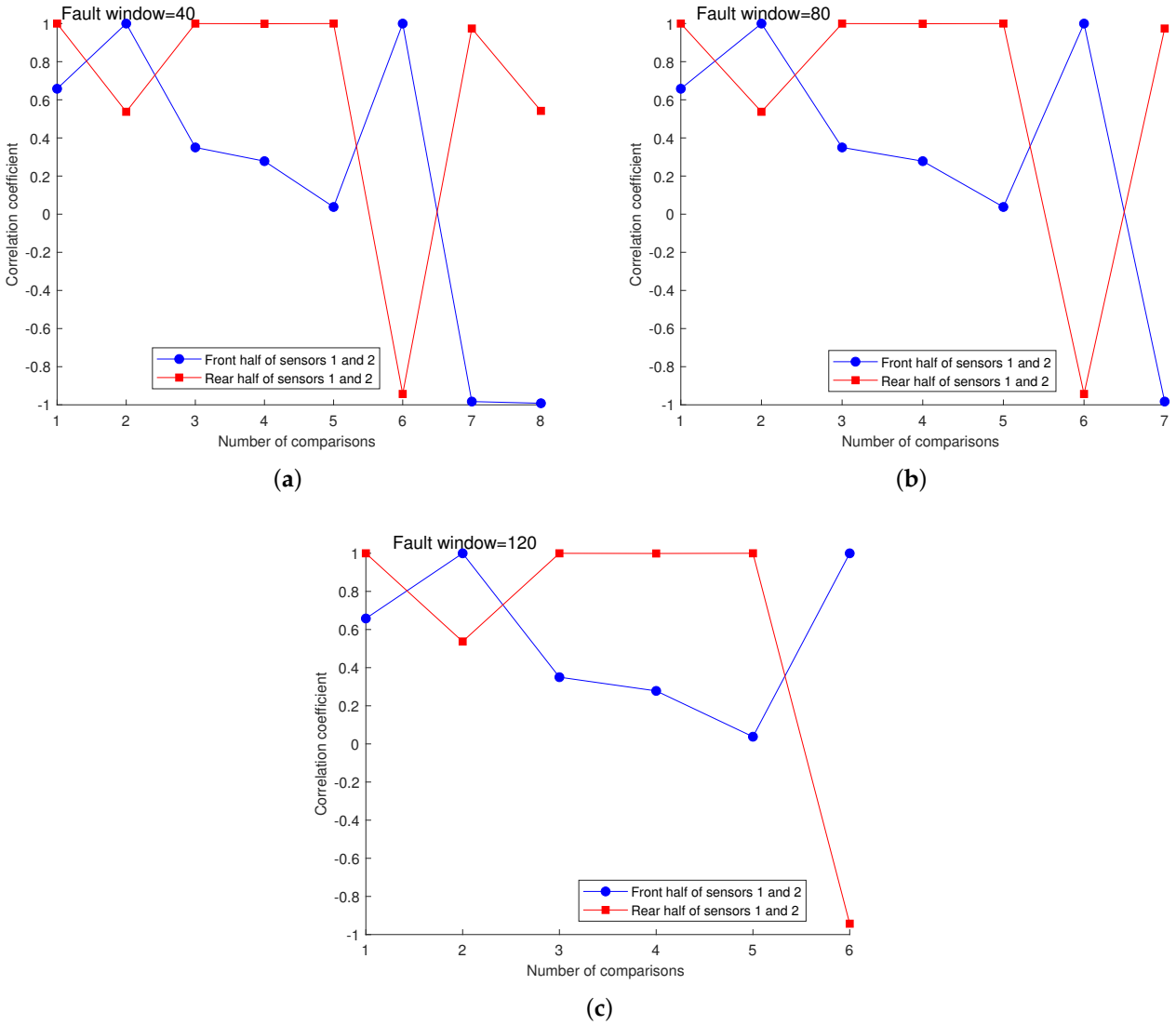


Figure 7. Fault window of ESC fault based on dichotomy correlation coefficient method. (**a**) Fault window size is 40; (**b**) fault window size is 80; (**c**) fault window size is 120.

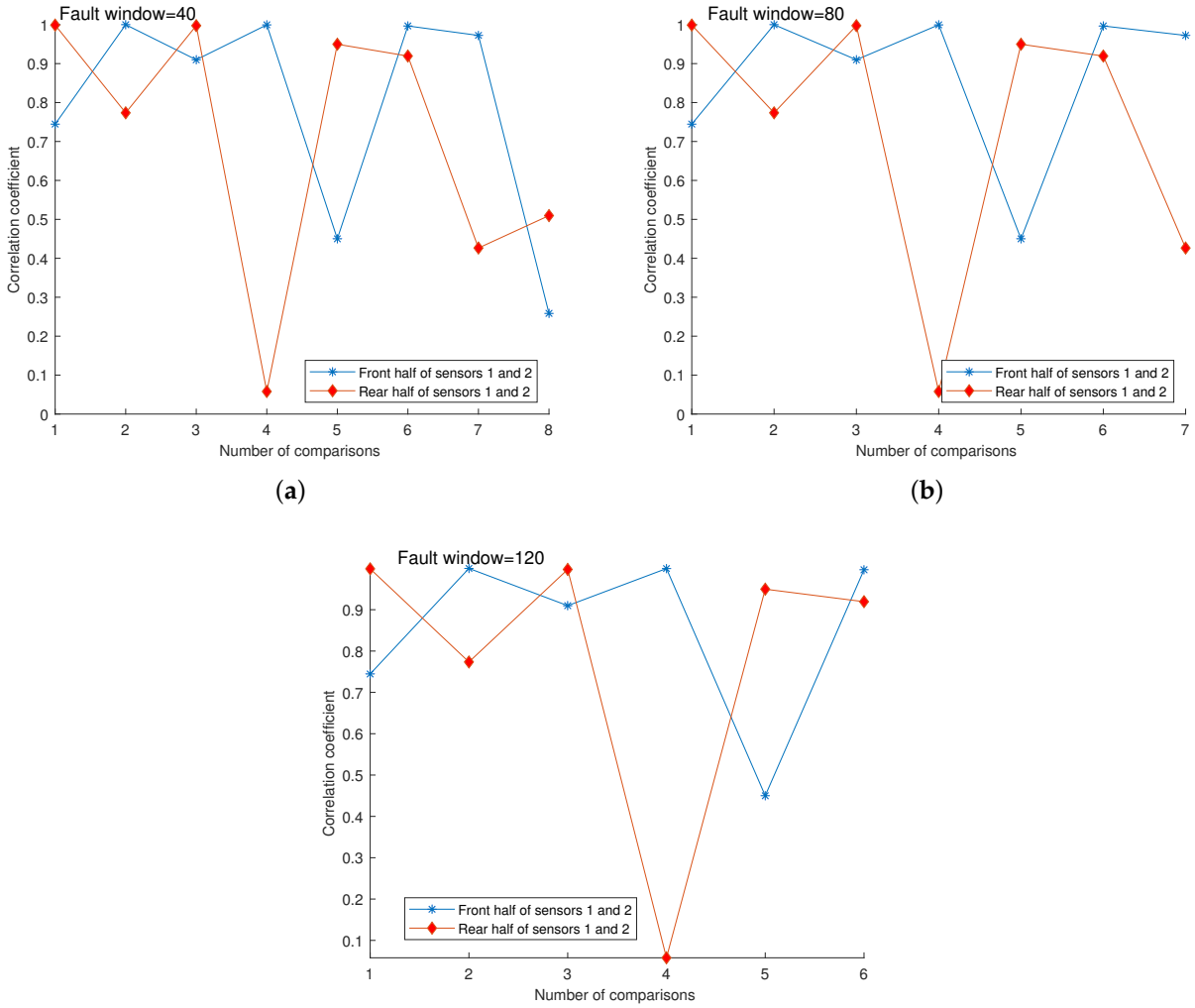


Figure 8. Fault window of ISC fault based on dichotomy correlation coefficient method. (**a**) Fault window size is 40; (**b**) fault window size is 80; (**c**) fault window size is 120.

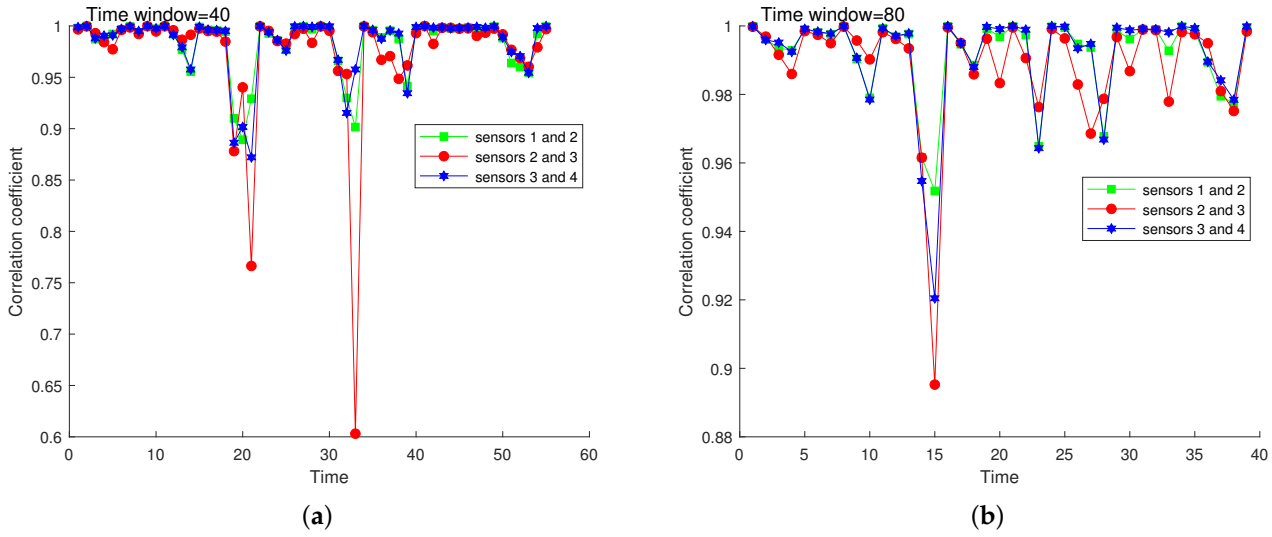
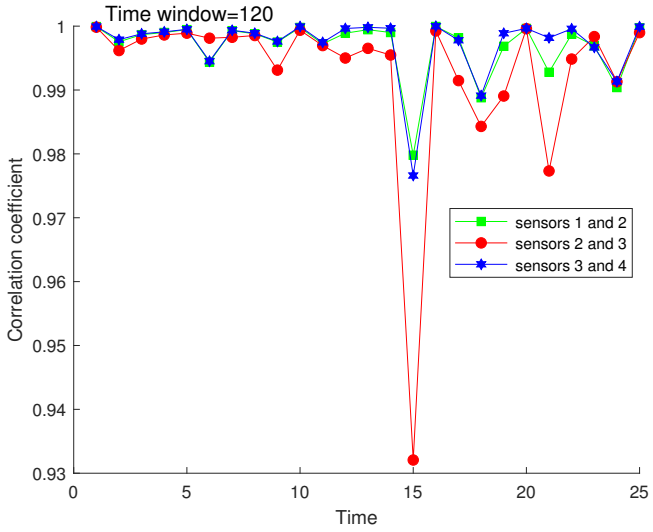


Figure 9. *Cont*.



(**c**)

Figure 9. Fault window of contact fault based on correlation coefficient method of time window. (**a**) Fault window size is 40; (**b**) fault window size is 80; (**c**) fault window size is 120.

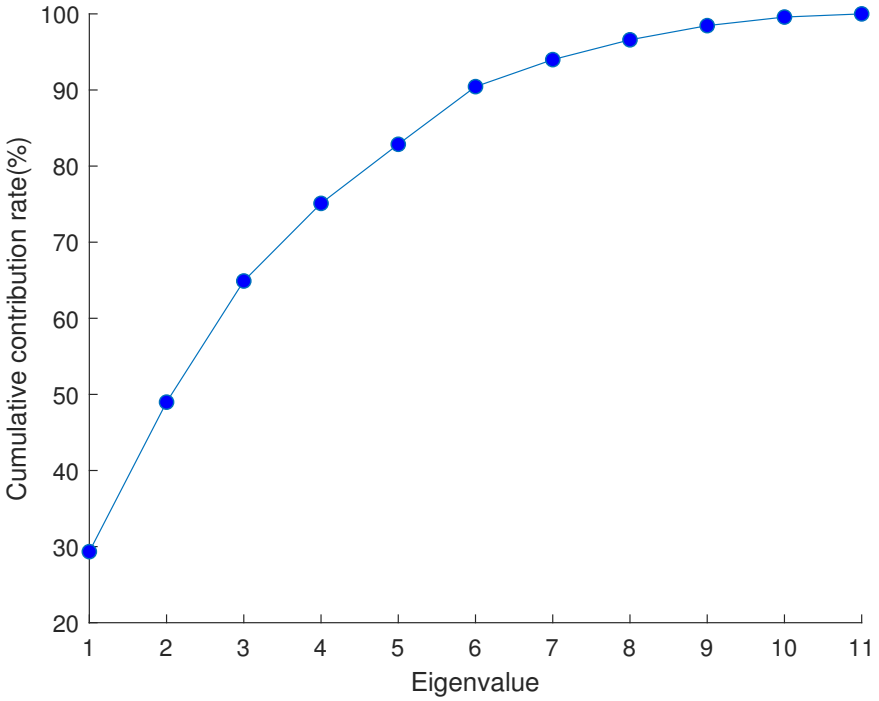


Figure 10. Accumulation rate of principal components.

4.3. Fault Classification

In this experiment, four types of data are classified, including ESC fault data, ISC fault data, contact fault data, and normal data. Because the battery system is highly nonlinear, the radial basis function kernel function is used as the kernel function of LSSVM. The maximum number of iterations of the classification model is set to 100. Since LSSVM is a binary classification model, considering the actual situation of lithium-ion battery fault diagnosis, $n(n-1)/2$ LSSVM classifiers will be established. In the LSSVM model, the regularization parameter γ and the kernel parameter σ determine its classification performance. The regularization parameter γ determines the model error and generalization ability, and the

kernel parameter σ reflects the complexity of the distribution of the training sample data in the high-dimensional feature space. Although these two parameters are so important, they are not completely related to the performance of LSSVM theoretically. Therefore, this paper uses the GWO algorithm to find the regularization parameter γ and the kernel parameter σ. The optimization idea of the LSSVM based on the GWO algorithm is as follows. Firstly, the number of the gray wolf population is initialized to 20 and the maximum iteration number of the algorithm is 100. An initial population position is randomly generated in the range of 0.01 to 1000. Additionally, a prey position parameter and a search distance parameter are initialized. Then the success rate of the training set is used as the fitness function to calculate the fitness of the individual gray wolves in turn, and the top three wolves with the best fitness are saved as α, β, and δ. The position of the gray wolf population is updated with a position updating formula. The convergence coefficient, the prey position parameter, and the hunting distance parameter are updated. The fitness is calculated, and the obtained fitness value is compared with the historical optimal fitness value, so as to obtain the optimal value. Iterations are performed again until the maximum number of iterations is reached. Finally, the optimal value obtained by the algorithm is assigned to the regularization parameter γ and the kernel parameter σ to construct the LSSVM classification model, which improves the classification accuracy of the LSSVM.

In this experiment, the fault type with the highest classification probability is selected as the predicted fault type. The k-fold cross-validation method can estimate the performance of the model more accurately by dividing the original training set into multiple validation sets. The GWO-LSSVM model was evaluated by k = 10 cross-validation. As can be seen from Figure 11, the classification accuracy of the test set ranged from 85% to 100% and the average accuracy is 94.75%.

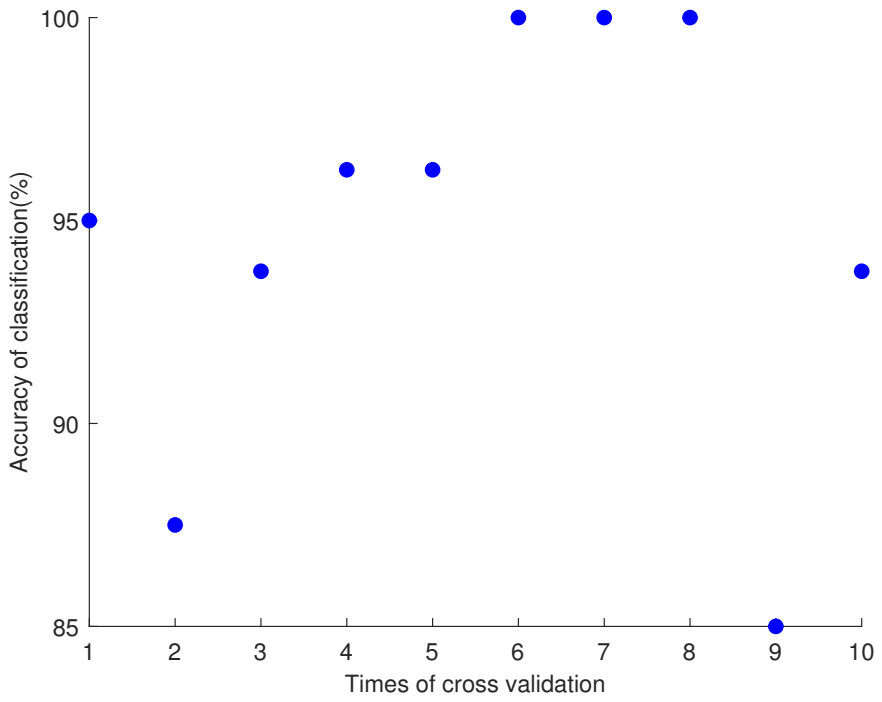


Figure 11. The accuracy rate of 10-fold cross-validation.

4.4. Comparison of Classification Model Performance

In order to evaluate the performance of the utilized classification models, this section chooses the support vector machine, adaptive boosting method (Adaboost), and Naive Bayesian Classifier (NBC) as comparison models. The sample data are divided into a training set and a test set. Each model is tested 10 times, with the test set accuracy recorded and the average accuracy calculated. The average accuracy for each model is shown in

Table 5. The Support Vector Machine is a binary classification model, but this test is a multi-classification problem. Therefore, $n(n-1)/2$ one-to-one classifiers are established, the radial basis function is selected as the kernel function, and optimal parameters are chosen through the gradient descent method. Adaboost is an ensemble learning model whose basic idea is to combine multiple weak classifiers into a strong classifier. Taking into account the model cost, 100 weak classifiers are constructed. The decision tree is chosen as the weak classifier. The decision tree takes internal nodes as attributes, branches as decision rules, and leaves as results. NBC is a classification algorithm grounded on Bayes' theorem. It calculates the prior and likelihood probabilities of the training set data, followed by the probabilities of the test set data. The highest probability is chosen as the final result. Discrete wavelet packet transform (DWPT) and relevance vector machine (RVM) constitute the fault diagnosis model. DWPT processes correlation sequence data and RVM classifies fault. Finally, classification results are obtained to calculate classification success rate [28].

SVM is sensitive to kernel function and initial parameters, and has higher computational complexity than GWO-LSSVM. The classification performance of the Adaboost model is determined by weak classifiers, but too many weak classifiers will not only increase the complexity of the model, but also may cause overfitting problems. The NBC model is based on the assumption that the features are independent of each other. However, in the fault diagnosis of a lithium-ion battery, there is a correlation between the fault features, which leads to a decline in classification performance. The DWPT-RVM model has problems of overfitting and high computational complexity in fault classification. As can be seen from Table 5, the GWO-LSSVM model has the highest average accuracy. This model has high efficiency in dealing with nonlinear classification problems, high robustness to initial parameters, and low computational cost.

Table 5. The average accuracy of fault classification of GWO-LSSVM,SVM, Adaboost, NBC, and DWPT-RVM.

Type	GWO-LSSVM	SVM	Adaboost	NBC	DWPT-RVM
Fault classification	94.67%	82.64%	85.65%	73.91%	90.33%

5. Conclusions

This paper has presented a fault diagnosis method for lithium-ion batteries based on the double fault window location and GWO-LSSVM classification model. The method has solved the problems of fault location and fault type identification of the series lithium-ion battery pack. Firstly, the battery voltage has been measured from the interleaved topology, then the battery voltage has been decomposed by using the ICEEMDAN to obtain the IMFs and the residual term. Noise has been eliminated through the reconstruction of the IMFs, and in addition, adding the IMFs and the residual terms has created a new voltage data sequence. Subsequently, the secondary fault window location model has been employed to determine the fault location. The fault features of IMFs have been extracted by PCA and classified using the GWO-LSSVM classification model. Finally, the fault injection platform is constructed, and experiments are carried out for various types of faults to obtain experimental data. Experimental results demonstrate that the fault diagnosis accuracy is 94.67%. The proposed method significantly enhances both the speed of fault location and the accuracy of diagnosis compared to existing methods.

Because the fault characteristics of different faults are different, using the same classification model to diagnose multiple faults will affect the accuracy of diagnosis. Considering the focus of different classification algorithms and the difference in the accuracy of different faults in the actual classification process, there is still a gap in the robustness of the classification model used in this paper. In addition, the sampling frequency also affects data validity and model computation time. Our future work will explore the similarity of fault characteristics of different faults and investigate the optimal classification models corresponding to different faults.

Author Contributions: Conceptualization, X.S.; methodology, X.S.; software, X.S.; validation, X.S.; formal analysis, X.S. and S.L.; investigation, X.S. and M.L.; resources, S.L.; data curation, X.S.; writing—original draft preparation, X.S.; writing—review and editing, X.S. and S.L.; visualization, X.S. and S.L.; supervision,X.S.; project administration, X.S. and S.L.; funding acquisition, S.L. All authors have read and agreed to the published version of the manuscript.

Funding: This research was funded by the National Natural Science Foundation of China (61773074) and the Key Project of Education Department of Liaoning Province (LJKZZ20220118).

Data Availability Statement: Data are contained within the article.

Conflicts of Interest: The authors declare no conflicts of interest.

Abbreviations

The following abbreviations are used in this manuscript:

EMD	empirical mode decomposition
ICEEMDAN	improved complete ensemble empirical mode decomposition with the adaptive noise
IMF	intrinsic mode function
GWO	gray wolf optimization
LSSVM	least squares support vector machine
SVM	support vector machin
ESC	external short circuit
ISC	internal short circui
BMS	battery management system
GWO-LSSVM	east squares support vector machine-grey wolf optimizatio
PCA	principal component analysis

References

1. Boddapati, V.; Kumar, A.R.; Daniel, S.A.; Padmanaban, S. Design and prospective assessment of a hybrid energy-based electric vehicle charging station. *Sustain. Energy Technol. Assessments* **2022**, *53*, 102389. [CrossRef]
2. Orošnjak, M.; Brkljač, N.; Šević, D.; Čavić, M.; Oros, D.; Penčić, M. From predictive to energy-based maintenance paradigm: Achieving cleaner production through functional-productiveness. *J. Clean. Prod.* **2023**, *408*, 137177. [CrossRef]
3. Yu, Q.; Wang, C.; Li, J.; Xiong, R.; Pecht, M. Challenges and outlook for lithium-ion battery fault diagnosis methods from the laboratory to real world applications. *eTransportation* **2023**, *17*, 100254. [CrossRef]
4. Tran, H.G.; Ton-That, L.; Thao, N.G.M. Lagrange Multiplier-Based Optimization for Hybrid Energy Management System with Renewable Energy Sources and Electric Vehicles. *Electronics* **2023**, *12*, 4513. [CrossRef]
5. Cai, H.; Hao, X.; Jiang, Y.; Wang, Y.; Han, X.; Yuan, Y.; Zheng, Y.; Wang, H.; Ouyang, M. Degradation Evaluation of Lithium-Ion Batteries in Plug-In Hybrid Electric Vehicles: An Empirical Calibration. *Batteries* **2023**, *9*, 321. [CrossRef]
6. Xiong, R.; Sun, W.; Yu, Q.; Sun, F. Research progress, challenges and prospects of fault diagnosis on battery system of electric vehicles. *Appl. Energy* **2020**, *279*, 115855. [CrossRef]
7. Xiong, R.; Ma, S.; Li, H.; Sun, F.; Li, J. Toward a Safer Battery Management System: A Critical Review on Diagnosis and Prognosis of Battery Short Circuit. *iScience* **2020**, *23*, 101010. [CrossRef] [PubMed]
8. Sun, Y.; Yuan, Y.; Lu, L.; Han, X.; Kong, X.; Wang, H.; Ouyang, M.; Gao, P.; Zheng, H.; Wang, K. A comprehensive research on internal short circuits caused by copper particle contaminants on cathode in lithium-ion batteries. *eTransportation* **2022**, *13*, 100183. [CrossRef]
9. Huang, L.; Liu, L.; Lu, L.; Feng, X.; Han, X.; Li, W.; Zhang, M.; Li, D.; Liu, X.; Sauer, D.U.; et al. A review of the internal short circuit mechanism in lithium-ion batteries: Inducement, detection and prevention. *Int. J. Energy Res.* **2021**, *45*, 15797–15831. [CrossRef]
10. Zhang, G.; Wei, X.; Tang, X.; Zhu, J.; Chen, S.; Dai, H. Internal short circuit mechanisms, experimental approaches and detection methods of lithium-ion batteries for electric vehicles: A review. *Renew. Sustain. Energy Rev.* **2021**, *141*, 110790. [CrossRef]
11. Zhu, J.; Wierzbicki, T.; Li, W. A review of safety-focused mechanical modeling of commercial lithium-ion batteries. *J. Power Sources* **2018**, *378*, 153–168. [CrossRef]
12. Hu, X.; Zhang, K.; Liu, K.; Lin, X.; Dey, S.; Onori, S. Advanced Fault Diagnosis for Lithium-Ion Battery Systems: A Review of Fault Mechanisms, Fault Features, and Diagnosis Procedures. *IEEE Ind. Electron. Mag.* **2020**, *14*, 65–91. [CrossRef]
13. Roy, P.K.; Shahjalal, M.; Shams, T.; Fly, A.; Stoyanov, S.; Ahsan, M.; Haider, J. A Critical Review on Battery Aging and State Estimation Technologies of Lithium-Ion Batteries: Prospects and Issues. *Electronics* **2023**, *12*, 4105. [CrossRef]
14. Lai, X.; Jin, C.; Yi, W.; Han, X.; Feng, X.; Zheng, Y.; Ouyang, M. Mechanism, modeling, detection, and prevention of the internal short circuit in lithium-ion batteries: Recent advances and perspectives. *Energy Storage Mater.* **2021**, *35*, 470–499. [CrossRef]

15. Yang, S.; Cheng, H.; Wang, M.; Lyu, M.; Gao, X.; Zhang, Z.; Cao, R.; Li, S.; Lin, J.; Hua, Y.; et al. Multi-scale Battery Modeling Method for Fault Diagnosis. *Automot. Innov.* **2022**, *5*, 400–414. [CrossRef]
16. Wang, X.; Wei, X.; Zhu, J.; Dai, H.; Zheng, Y.; Xu, X.; Chen, Q. A review of modeling, acquisition, and application of lithium-ion battery impedance for onboard battery management. *eTransportation* **2021**, *7*, 100093. [CrossRef]
17. Yu, Q.; Dai, L.; Xiong, R.; Chen, Z.; Zhang, X.; Shen, W. Current sensor fault diagnosis method based on an improved equivalent circuit battery model. *Appl. Energy* **2022**, *310*, 118588. [CrossRef]
18. Wei, J.; Dong, G.; Chen, Z. Lyapunov-Based Thermal Fault Diagnosis of Cylindrical Lithium-Ion Batteries. *IEEE Trans. Ind. Electron.* **2020**, *67*, 4670–4679. [CrossRef]
19. Xiong, R.; Yu, Q.; Shen, W.; Lin, C.; Sun, F. A Sensor Fault Diagnosis Method for a Lithium-Ion Battery Pack in Electric Vehicles. *IEEE Trans. Power Electron.* **2019**, *34*, 9709–9718. [CrossRef]
20. Dey, S.; Perez, H.E.; Moura, S.J. Model-Based Battery Thermal Fault Diagnostics: Algorithms, Analysis, and Experiments. *IEEE Trans. Control. Syst. Technol.* **2019**, *27*, 576–587. [CrossRef]
21. Gao, Z.; Cecati, C.; Ding, S.X. A Survey of Fault Diagnosis and Fault-Tolerant Techniques—Part II: Fault Diagnosis With Knowledge-Based and Hybrid/Active Approaches. *IEEE Trans. Ind. Electron.* **2015**, *62*, 3768–3774. [CrossRef]
22. Wu, C.; Zhu, C.; Ge, Y. A New Fault Diagnosis and Prognosis Technology for High-Power Lithium-Ion Battery. *IEEE Trans. Plasma Sci.* **2017**, *45*, 1533–1538. [CrossRef]
23. Tran, M.-K.; Fowler, M. A Review of Lithium-Ion Battery Fault Diagnostic Algorithms: Current Progress and Future Challenges. *Algorithmse* **2020**, *13*, 62. [CrossRef]
24. Xia, B.; Nguyen, T.; Yang, J.; Mi, C. The improved interleaved voltage measurement method for series connected battery packs. *J. Power Sources* **2016**, *334*, 12–22. [CrossRef]
25. Xia, B.; Shang, Y.; Nguyen, T.; Mi, C. A correlation based fault detection method for short circuits in battery packs. *J. Power Sources* **2017**, *337*, 1–10. [CrossRef]
26. Kang, Y.; Duan, B.; Zhou, Z.; Shang, Y.; Zhang, C. Online multi-fault detection and diagnosis for battery packs in electric vehicles. *Appl. Energy* **2020**, *259*, 114170. [CrossRef]
27. Kang, Y.; Duan, B.; Zhou, Z.; Shang, Y.; Zhang, C. A multi-fault diagnostic method based on an interleaved voltage measurement topology for series connected battery packs. *J. Power Sources* **2019**, *417*, 132–144. [CrossRef]
28. Yang, Y.; Lun, S.; Xie, J. Multi-fault diagnosis for battery pack based on adaptive correlation sequence and sparse classification model. *J. Energy Storage* **2022**, *46*, 103889. [CrossRef]
29. Zhou, J.; Wu, Z.; Zhang, S.; Wang, P. A Fault Diagnosis Method for Power Battery Based on Multiple Model Fusion. *Electronics* **2023**, *12*, 2724. [CrossRef]
30. Jiang, J.; Li, T.; Chang, C.; Yang, C.; Liao, L. Fault diagnosis method for lithium-ion batteries in electric vehicles based on isolated forest algorithm. *J. Energy Storage* **2022**, *50*, 104177. [CrossRef]
31. Ma, M.; Li, X.; Gao, W.; Sun, J.; Wang, Q.; Mi, C. Multi-fault diagnosis for series-connected lithium-ion battery pack with reconstruction-based contribution based on parallel PCA-KPCA. *Appl. Energy* **2022**, *324*, 119678. [CrossRef]
32. Xu, C.; Li, L.; Xu, Y.; Han, X.; Zheng, Y. A vehicle-cloud collaborative method for multi-type fault diagnosis of lithium-ion batteries. *eTransportation* **2022**, *12*, 100172. [CrossRef]
33. Dliou, A.; Elouaham, S.; latif, R.; Laaboubi, M.; Zougagh, H.; Saddik, A. Denoising Ventricular tachyarrhythmia Signal. In Proceedings of the 2018 9th International Symposium on Signal, Image, Video and Communications (ISIVC), Rabat, Morocco, 27–30 November 2018; pp. 124–128.
34. Elouaham, S.; Dliou, A.; Elkamoun, N.; Latif, R.; Said, S.; Zougagh, H.; Khadiri, K. Denoising electromyogram and electroencephalogram signals using improved complete ensemble empirical mode decomposition with adaptive noise. *Indones. J. Electr. Eng. Comput. Sci.* **2021**, *2*. [CrossRef]
35. Colominas, M.A.; Schlotthauer, G.; Torres. M.E. Improved complete ensemble EMD: A suitable tool for biomedical signal processing. *Biomed. Signal Process. Control.* **2014**, *14*. 19–29. [CrossRef]
36. Mirjalili, S.; Mirjalili, S.M.; Lewis, A.D. Grey Wolf Optimizer. *Adv. Eng. Softw.* **2014**, *69*, 46–61. [CrossRef]

Disclaimer/Publisher's Note: The statements, opinions and data contained in all publications are solely those of the individual author(s) and contributor(s) and not of MDPI and/or the editor(s). MDPI and/or the editor(s) disclaim responsibility for any injury to people or property resulting from any ideas, methods, instructions or products referred to in the content.